The 11th Canadian Conference on Earthquake Engineering
Canadian Association for Earthquake Engineering

NUMERICAL MODELLING OF REINFORCED CONCRETE BLOCK STRUCTURAL WALLS WITH BOUNDARY ELEMENTS UNDER SEISMIC LOADING

Mohamed Ezzeldin
PhD Candidate, McMaster University, Department of Civil Engineering, Canada.
ezzeldms@mcmaster.ca

Lydell Wiebe
Assistant Professor, McMaster University, Department of Civil Engineering, Canada.
wiebel@mcmaster.ca

Wael El-Dakhakhni
Martini, Mascarin and George Chair in Masonry Design, McMaster University, Canada.
eldak@mcmaster.ca

ABSTRACT: Reinforced masonry (RM) walls typically have single-leg horizontal reinforcement and a single layer of vertical reinforcement because of practical limitations associated with masonry unit configuration and construction. As such, little or no confinement is usually available at the critical wall compression zones of RM walls. This reinforcing arrangement in RM may lead to instability of the toes under high inelastic strains in the vertical bars during cyclic loading. Boundary elements allow closed ties to be formed and multiple layers of vertical bars to be accommodated, thus providing a confining reinforcing cage within the RM wall. This in turn prevents the vertical wall reinforcement from buckling, thus enhancing the overall performance of the RM wall seismic force resisting system. Very little research has been carried out on modelling RM walls with boundary elements because of the lack of experimental data. In this paper, OpenSees is used to create macro models to simulate the in-plane response of RM walls with boundary elements under cyclic loading. The models are validated against the results of experimental tests on RM walls with boundary elements under cyclic in-plane lateral loads. This paper demonstrates that simple models, with minimal calibration for the plastic hinge length only, can capture the cyclic response, including energy dissipation and degradation of strength and stiffness, very well.

1. Introduction

Rectangular fully grouted RM shear walls have been widely used as seismic force resisting systems because of their inherently large lateral stiffness and load resistance. Due to the concrete block unit configuration associated with the traditional rectangular RM shear walls, single horizontal ties and a single layer of vertical reinforcement are typically used. This arrangement provides almost no confinement at the wall ends, and it may lead to instability of the compression zone during cyclic loading. However, using boundary elements in a rectangular RM wall allows a closed tie to replace the typical 180° hook formed by the horizontal shear reinforcement. This also accommodates multiple layers of vertical bars in the end zone, providing a reinforcing cage that confines the concrete in that region and that delays the buckling of the walls' vertical reinforcement. Relative to rectangular RM walls, this enables the compression reinforcement to remain effective beyond the point where the concrete cover has spalled. The behaviour of RM walls with boundary elements is characterized by a small compression zone, which

decreases the curvature at the yield of the vertical reinforcement and increases the ultimate curvature relative to a wall without boundary elements (e.g. a rectangular wall). Together, these two effects increase the curvature ductility, and therefore the displacement ductility (Banting et al. 2012). Very little research has been carried out on modelling of RM walls without or with boundary elements under lateral load due to the lack of the experimental data. The behaviour of these walls depends on the behaviour of several materials that have different characteristics (e.g. blocks, reinforcement, grout), making the nonlinear analysis of such walls challenging. Consequently, there is a need to develop a numerical model of these shear walls that is both accurate and simple enough to be included as a part of a full building model.

This paper develops a 2D simplified numerical model in OpenSees, using displacement-based beam column elements, to simulate the behaviour of RM shear walls with boundary elements under cyclic loading. A description of the experimental program used to validate the proposed modelling technique is presented, followed by a detailed description of the 2D model. The model is then validated against the experimental results.

2. Background on Numerical Models of RM Shear Walls

Limited studies have been conducted to simulate the nonlinear behaviour of RM shear walls. These studies can be categorized under two levels of refinement: 1) micro-modelling, where each component of the masonry wall is modelled individually, and 2) macro-modelling, where an equivalent material is used to model the masonry wall as a larger unit.

2.1 Micro-Modelling

Micro-modelling is a well-known approach for small structures. In a micro model, the structure is discretized into a finite number of small elements interconnected at a finite number of nodes. The main elements used in this kind of modelling are masonry, mortar joint, masonry-mortar interface and steel elements. Since each element can be modelled in detail, a micro-modelling strategy is often preferred for understanding the local behaviour of masonry failures for small structural elements (e.g. assemblages). Modern plasticity concepts have been used to develop an interface cap model, capable of capturing masonry failure mechanisms, including tensile cracking, frictional slip and crushing along interfaces (Lourenço et al. 1997). This approach was extended to study the individual fracture of mortar and bricks (Guinea et al. 2000).

Although micro-modelling can produce very accurate results, it is computationally expensive because the relatively small dimensions of the elements require a large number of nodes. Therefore, it may not be practical for inelastic response history analysis of complete masonry structures.

2.2 Macro-Modelling

Macro-modelling is based on representing the overall structure with a smaller number of elements, each of which has properties that are equivalent to the sum of its components. It is commonly used for large structures to study properties such as energy dissipation, structural deformation and strength capacity. This method does not require the level of detailed representation used for micro-modelling, so it is more practical for analytical and numerical modelling of full masonry structures. Masonry walls have been modelled as a homogenous medium, overlaid with two sets of planes of weakness, representing head and bed joints, and two sets of reinforcement (El-Dakhakhni et al. 2006). In order to capture the different failure modes of masonry-infilled frames, a combination of the smeared and discrete crack approaches has been used (Stavridis et al. 2010).

The previous models all require a high level of detail, resulting in a high level of computational effort. Therefore, there is still a need to develop simplified models that can simulate the behaviour of RM structures based on material and geometric properties. Moreover, whereas the previous models concentrate on traditional rectangular RM shear walls, no work has been done to model RM shear walls with boundary elements under seismic loading.

3. Experimental Program

The numerical model developed in this paper will be validated against the test results of two RM shear walls (specimens W3 and W6) that were reported by Shedid et al. (2010). That study focused on the cyclic flexural response of half-scale fully grouted RM shear walls with boundary elements. A brief overview of the experimental program is presented in this section.

3.1 Test Matrix

Table 1 summarizes the wall dimensions, aspect ratios and reinforcement details, where φ_v and φ_h are the vertical and horizontal bar diameters, respectively. The vertical and horizontal reinforcement ratios are denoted by ρ_v and ρ_h, respectively. This experimental program was selected to validate the numerical model because it includes walls with different aspect ratios, 2.22 and 1.47.

Table 1 – Summary of wall dimensions and reinforcement details.

Wall ID.	Length (mm)	Height (mm)	Vertical Reinforcement		Horizontal Reinforcement		Aspect Ratio
			φ_v (mm)	ρ_v %	φ_h (mm)	ρ_h %	
W3	1802	3990	11.30	0.55	5.68	0.30	2.22
W6	1802	2660	11.30	0.55	5.68	0.60	1.47

Fig. 1 shows that the half-scale walls W3 and W6 have three and two storeys, respectively, with a reinforced concrete slab at each storey level. All walls were built on a concrete foundation having a height and width of 400 mm and 1100 mm, respectively. Fig. 2 shows that the web of each wall was 90 mm thick and the boundary elements used an additional block at each wall end to increase the end thickness to 185 mm over a length of 185 mm (1 block). The wall was reinforced with 3M10 (11.30 mm) vertical bars along the web and 4M10 bars in each boundary element. The horizontal reinforcement, consisting of one and two D4 bars (5.68 mm) for walls W3 and W6, respectively, was placed at every course (90 mm spacing) and formed 180° hooks around the outmost vertical reinforcement. In addition, closed ties were provided around the four end bars to ensure the anchorage of the horizontal reinforcement inside the boundary element.

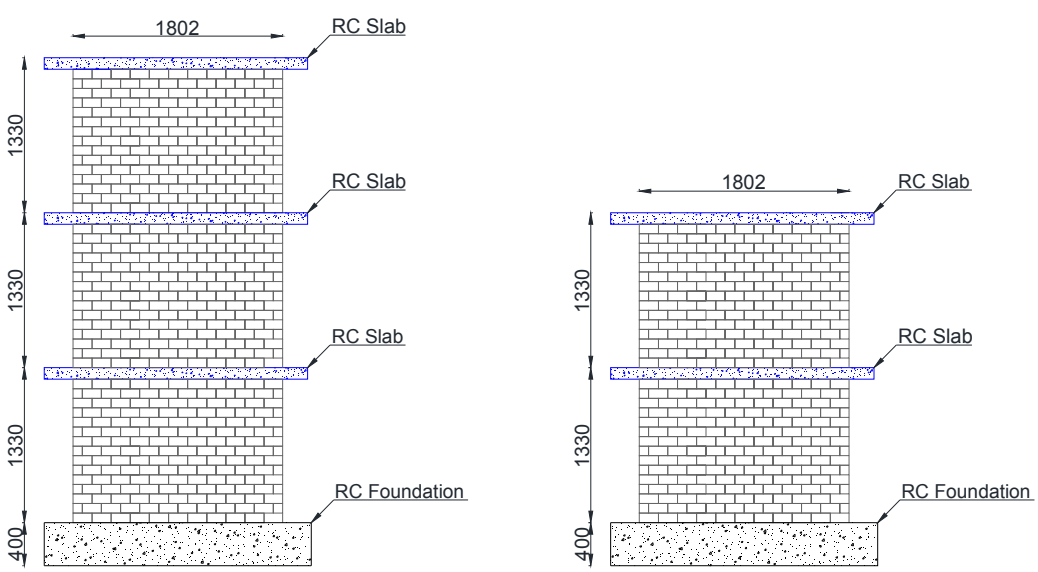

(a) W3 (aspect ratio=2.22) (b) W6 (aspect ratio=1.47)

Fig. 1 – Wall Layouts (All dimensions are in mm)

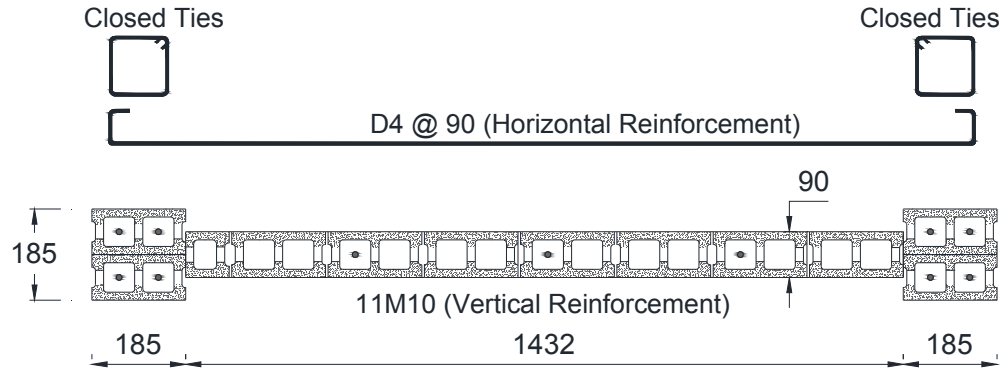

Fig. 2 – Cross-Section and Reinforcement Details of W3 and W6 (All Dimensions are in mm)

3.2 Materials

The half-scale blocks were 185 mm long, 90 mm thick and 90 mm tall. The average compressive strength of masonry-grout prisms was 18.8 MPa, while the average yield strengths of vertical and horizontal bars were 495 MPa and 534 MPa, respectively (Shedid et al. 2010).

3.3 Test Setup

The setup for cyclic testing included a reusable base that was fixed to the structural floor of the laboratory by four post-tensioned steel rods. The wall foundation was fixed to the reusable base using similar post-tensioned rods. The loading scheme for all tests consisted of a series of displacement-controlled loading cycles applied at the top of the walls to assess the strength and the stiffness degradation. The walls were cycled twice at each displacement level. To obtain information that included the post-peak behaviour, the displacements were increased until the specimen had achieved its maximum lateral load resistance and then reduced to approximately 80% of its maximum capacity (Shedid et al. 2010).

4. Numerical Modelling

4.1 Element Type and Size

In this paper, a two-dimensional (2D) model with displacement-based beam-column elements was developed using OpenSees to simulate the inelastic behaviour of the walls. Fig. 3 shows a schematic diagram of the model, including the distribution of nodes and elements. Displacement-based beam-column elements follow the standard finite element formulation, in which the element displacement field is derived from nodal displacements. The formulation of this element assumes a linear curvature distribution and a constant axial strain. The beam-column elements were assigned fiber sections that discretely modelled the reinforcement and masonry regions. Five Gauss integration points were used for each element.

The choice of element length is a very important aspect when displacement-based beam-column elements are used with distributed plasticity and strain-softening material laws. This is because of strain localization, in which the plastic deformation tends to concentrate in the first element above the base of the wall, while the adjacent elements remain elastic (Coleman and Spacone 2001, Ezzeldin et al. 2014). Because of strain localization, the numerical results are very sensitive to the length of the first element length above the base, which should be equal to the plastic hinge length. A large element length results in larger lateral load capacity of the wall and no strength degradation, whereas a smaller element length underestimates the lateral load capacity of the wall. The formula proposed by Bohl and Adebar (2011) to estimate the plastic hinge length is given in Equation 1. It is based on nonlinear finite element analysis results of 22 isolated reinforced concrete shear walls and was found to give a good estimate of the plastic hinge length, L_p, for RM shear walls with and without boundary elements (Ezzeldin et al. 2015). The formula is a function of the wall length, L_w, moment-shear ratio, Z, gross area of wall cross section, A_g, concrete compressive strength, f'_c, and axial compression, P:

$$L_p = (0.20L_w + 0.05Z)(1 - \frac{1.5P}{f'_c A_g}) \leq 0.80L_w \quad (1)$$

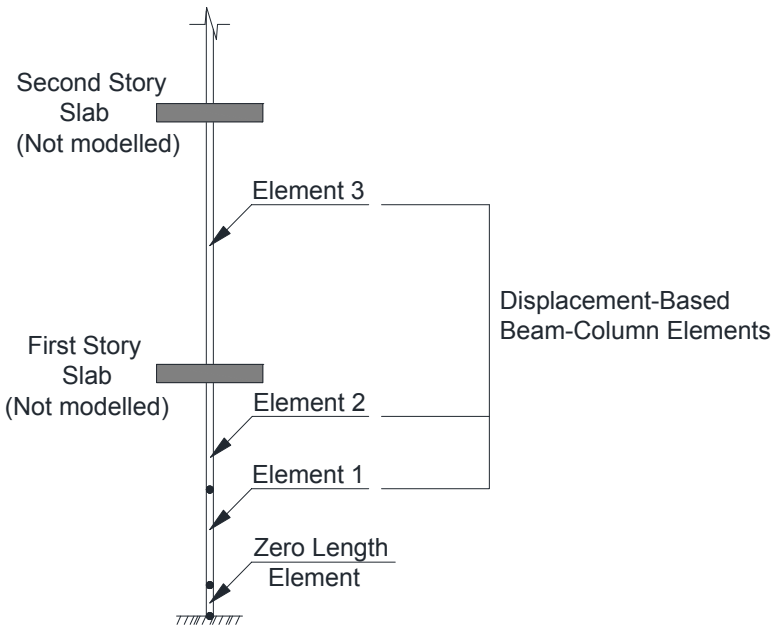

Fig. 3 – Schematic Diagram of the Model

4.2 Material Model for Masonry

Chang and Mander's model for concrete (Concrete 07) in OpenSees was used to model the masonry in this work. The Chang and Mander concrete model in OpenSees depends on the compressive strength, f'_m, the strain at the maximum compressive strength, ε_m, the elastic modulus, E_m, and other parameters that define strength and stiffness degradation. The strength and stiffness degradation parameters were taken according to the formulae reported in Chang et al. (1994). Unlike rectangular RM shear walls, RM walls with boundary elements have stirrups to confine the masonry and the vertical reinforcement near the extreme compression fiber. This confinement significantly enhances both the strength and the ductility of the compressed masonry zone (boundary element region). This was taken into consideration by assigning different material properties for the masonry inside the closed ties at the boundary element area. The model by Mander et al. (1988) was used to calculate the compressive strength, f'_{mc}, and the strain at maximum compressive strength, ε_{mc}, within the boundary element confined area:

$$f'_{mc} = f'_m(1 + k_1 x') \quad (2)$$

$$\varepsilon_{mc} = \varepsilon_m(1 + k_2 x') \quad (3)$$

k_1, k_2 and x' are factors that depend on the vertical and horizontal reinforcement ratios in the boundary elements. Fig. 4 shows the material distribution through the cross-section area of the walls. The reinforcing steel was modelled using a Giuffre-Menegotto-Pinto model available in OpenSees (Steel02). All of these properties and parameters were defined based on material characterization tests, without any need for calibration to the overall wall response.

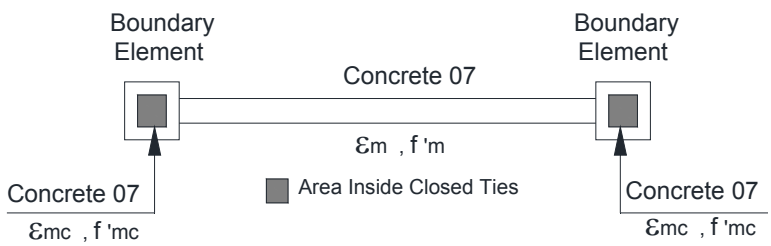

Fig. 4 – Material Distribution of RM Shear Walls with Boundary Elements in the model

4.3 Material Models for Reinforcement and Shear

The response of RM shear walls is affected by the buckling of longitudinal reinforcement in unconfined areas, such as the webs of walls with boundary elements. Bar buckling cannot be simulated directly using the Steel02 material in OpenSees, so it was simulated indirectly by taking the fracture strain of the vertical bars as 0.05 using the MinMax material option. This is about 50% of the fracture strain that was measured in direct tension tests, based on results reported by Rodriguez et al. (1999). The actual fracture strain of the bar was reported to be influenced by low-cycle fatigue, which depends on the loading history of the bar.

Strain penetration was modelled by using a zero-length element at the base, where the vertical reinforcement was replaced by the Bond_SP01 material in OpenSees. The total bar slip due to strain penetration is calculated in this model as a function of bar stress .

Shear behaviour was modelled using the Pinching4 material model with the section aggregator option to include the shear behavior of the wall within the flexural behavior of the fiber section. Three points are needed to define the response envelope of this Pinching4 material. The lateral force corresponding to the first flexural cracking and the uncracked shear stiffness were used to define the first point. The lateral force causing flexural yielding of the vertical reinforcement and the effective shear stiffness (20% of the uncracked shear stiffness) were selected to define the second point. Finally, the third point was defined using the ultimate lateral force and the post-yield shear stiffness (1% of the effective shear stiffness) (Waugh et al. 2008).

5. Comparison Between Numerical and Experimental Results

Fig. 5 shows that there is good agreement between the experimental hysteresis loops and the corresponding loops from the cyclic analysis using OpenSees. The model is able to simulate most relevant characteristics of the cyclic wall response, including the initial stiffness, peak load, stiffness degradation, strength deterioration, hysteretic shape and pinching behaviour at different drift levels. The following sections discuss these parameters in more detail.

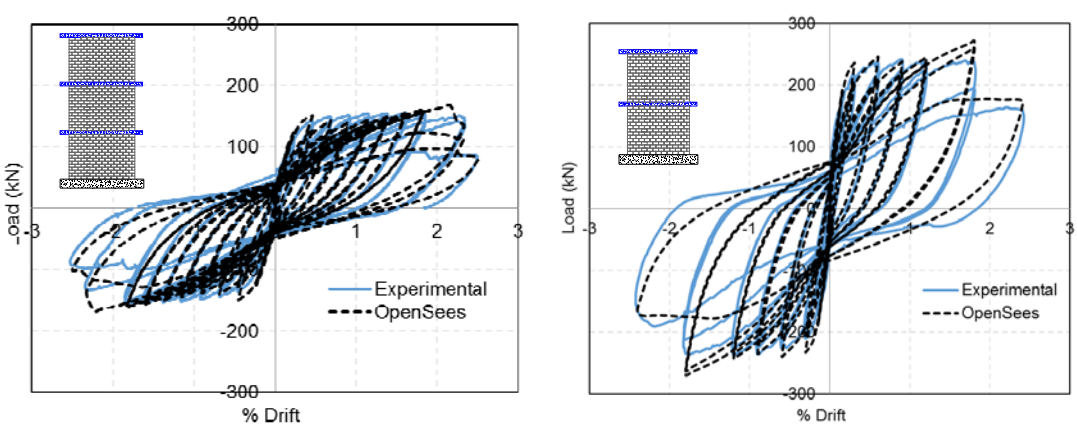

(a) Wall W3 (aspect ratio = 2.22). (b) Wall W6 (aspect ratio = 1.47).

Fig. 5 – Experimental and Numerical Hysteresis Loops of Wall W3 and Wall W6

5.1 Hysteretic Behaviour

Fig. 6 compares the individual the experimental and numerical hysteresis loops for Wall W3, using the first cycle at each drift level. The figure shows that the model can capture the loading and unloading stiffness, as well as the pinching behaviour. These ranges cover almost the entire portion of the load-displacement curve up to 80% strength degradation. Similar results were obtained for Wall W6, but graphs are not shown here.

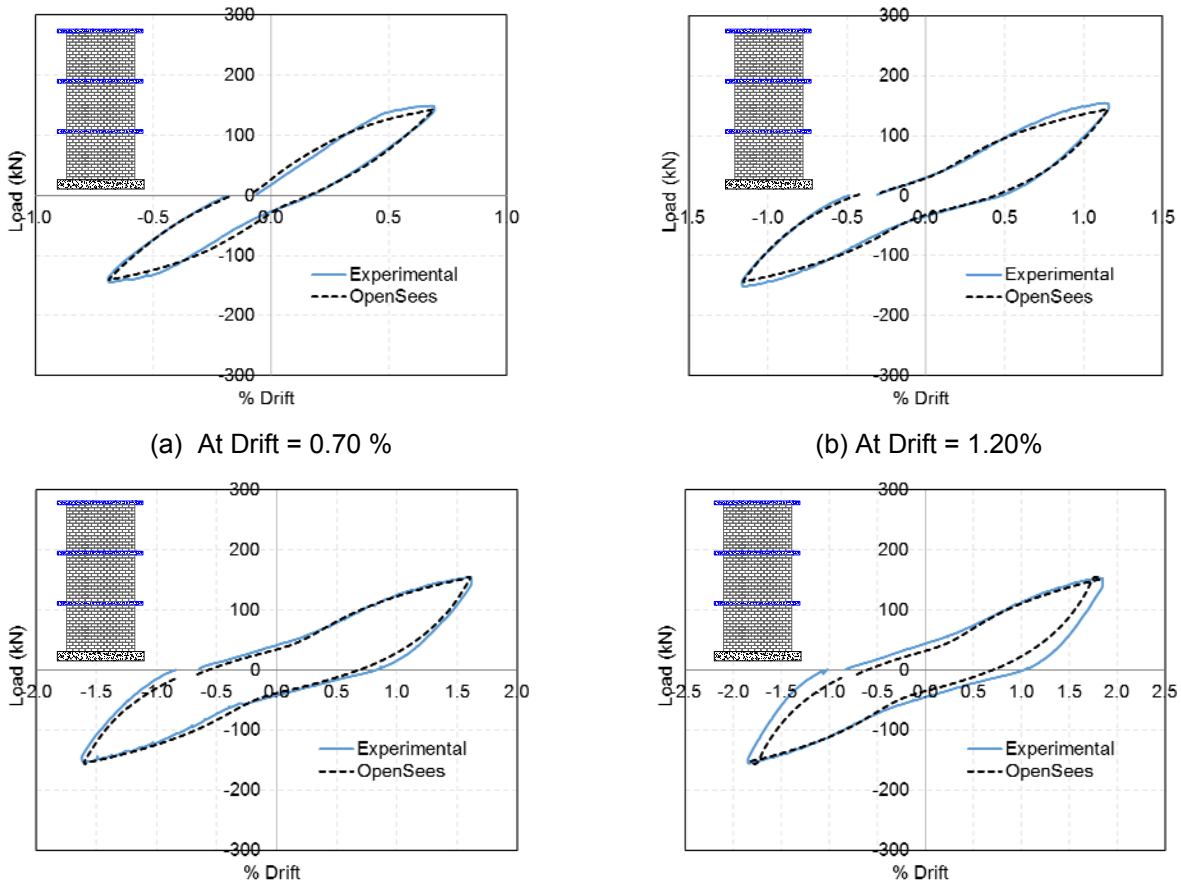

(a) At Drift = 0.70 %

(b) At Drift = 1.20%

(c) At Drift = 1.60%

(d) At Drift = 1.90%

Fig. 6 – Detailed Experimental and Numerical Hysteresis Loops of Wall W3 (Aspect Ratio=2.22)

5.2 Wall Capacity

The lateral capacity of Wall W3 was predicted very closely for most of the lateral drift levels, as shown in Fig. 7a. Relative to the experimental results, the maximum percentage of error in the lateral load either in push or pull directions is less than 9 and 12% in Walls W3 and W6, respectively.

5.3 Effective Stiffness

To assess the variation of stiffness with increased displacement, the effective stiffness was calculated according to the following formula, which is the ratio between the sum of the absolute maximum forces and the sum of the absolute maximum displacements in both directions for each loop:

$$K_{eff} = \frac{\left|F^{+}\right| + \left|F^{-}\right|}{\left|\Delta^{+}\right| + \left|\Delta^{-}\right|} \tag{4}$$

Fig. 7b shows that the numerical model captures the experimental results with a maximum error of 8 % for Wall W3. For Wall W6, the maximum difference between numerical and experimental effective stiffness at different drift ratios is less than 13%.

5.4 Energy Dissipation

Energy dissipation through hysteretic damping, E_d, is an important aspect in seismic design because it reduces the amplitude of the seismic response. Previous research showed that the envelope of the load-displacement hysteresis loops is relatively insensitive to the imposed displacement increments and to the number of cycles (Hose and Seible 1999). Therefore, the energy dissipation, E_d, is represented by the area enclosed by the load-displacement curve passing through the envelope values at each displacement level, as suggested by Hose and Seible (1999). Fig. 7c shows that the energy dissipation increased significantly at higher drift levels as the inelastic deformations in masonry and reinforcement increased compared to early stages of loading. The difference between the experimental and numerical results is less than 11% and 13% for Walls W3 and W6, respectively.

North American Codes quantify the energy dissipation within different systems through hysteric damping. The hysteretic damping can be described by an equivalent viscous damping ratio, ζ_{eq}, which is based on an equal area approach that represents the same amount of energy loss per loading cycle. According to Chopra (2000), the relationship between the dissipated energy, E_d, the stored strain energy, E_s, and the equivalent viscous damping ratio, ζ_{eq}, is given as:

$$\zeta_{eq} = \frac{E_d}{4\pi E_s} \tag{5}$$

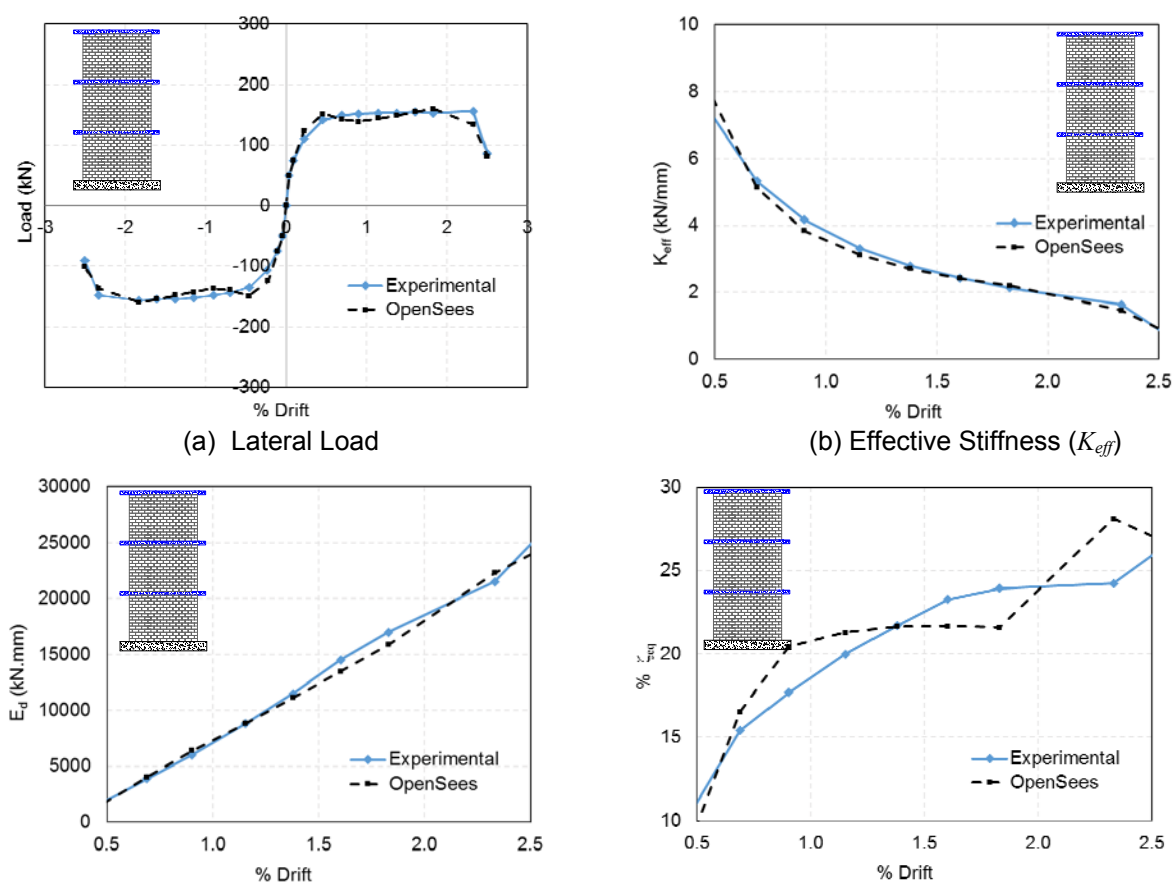

(a) Lateral Load

(b) Effective Stiffness (K_{eff})

(c) Energy Dissipation (E_d)

(d) Equivalent Viscous Damping (ζ_{eq})

Fig. 7 – Experimental and Numerical Response of Wall W3 (Aspect Ratio=2.22)

Fig. 7d summarizes the equivalent viscous damping ratios at different drift levels. The model captures the increase of equivalent viscous damping with loading with a maximum error of approximately 18% and 16% for Walls W3 and W6, respectively. The error in equivalent viscous damping is more than the error in energy dissipation because the model overestimates the energy dissipation, E_d, in some of the same cycles that it underestimates the elastic strain energy, E_s.

5.5 Displacement Ductility

Displacement ductility refers to the ability of the wall to deform beyond the initial yielding of the vertical reinforcement. There are many different definitions for the displacement ductility, since the real load-displacement behaviour of the walls is not elastic-perfectly-plastic. In this paper, the displacement ductility ($\mu_{\Delta}^{ep}{}_{0.8u}$) is defined as the ratio of the displacement associated with a degradation to 80% of the maximum strength to the effective yield displacement of an equivalent elastic-perfectly-plastic system that provides equal energy under the curve up to 80% strength degradation (Shedid et al. 2010). The experimental and numerical displacement ductility values are summarized in Table 2. The table shows that the model is able to estimate the displacement ductility of the walls to within a maximum error of 10%.

Table 2 – Summary of experimental and numerical displacement ductilities.

Wall ID (Aspect Ratio)	Push direction			Pull direction		
	$\mu_{\Delta}^{ep}{}_{0.8u}$ (Experiment)	$\mu_{\Delta}^{ep}{}_{0.8u}$ (OpenSees)	% Difference	$\mu_{\Delta}^{ep}{}_{0.8u}$ (Experiment)	$\mu_{\Delta}^{ep}{}_{0.8u}$ (OpenSees)	% Difference
W3 (AR=2.22)	7.8	8.2	+5.5	6.9	7.3	+6.1
W6 (AR=1.47)	9.0	9.8	+9.6	11.4	10.5	-7.9

6. Conclusions

This paper developed a simplified 2D numerical macro model using OpenSees to simulate the behaviour of reinforced masonry shear walls with boundary elements under cyclic loading. Data from an experimental test program was used to verify the proposed modelling technique, and it was found that this model is generally satisfactory in predicting the peak values of cyclic load of the experimental specimens, as well as the energy dissipation and ductility.

This paper demonstrated that reinforced masonry shear walls with boundary elements can be simulated using a macro model scale. Ongoing research seeks to verify the robustness of the model for different walls with different aspect ratios. Research is also underway to apply this modelling technique to understand the inelastic dynamic behaviour of reinforced concrete block shear walls with boundary elements under seismic loads.

7. Acknowledgments

The financial support for this project was provided through the Natural Sciences and Engineering Research Council (NSERC) of Canada. Support was also provided by the McMaster University Centre for Effective Design of Structures (CEDS), funded through the Ontario Research and Development Challenge Fund (ORDCF) of the Ministry of Research and Innovation (MRI) as well as the Canada Masonry Design Centre (CMDC).

8. References

BANTING, Bennett, EL-DAKHAKHNI, Wael, “Force-and Displacement-Based Seismic Performance Parameters for Reinforced Masonry Structural Walls with Boundary Elements”, *Journal of Structural Engineering*, Vol. 138, No. 12, December 2012, pp. 1477–1491.

BOHL, Alfredo, ADEBAR, Perry, “Plastic Hinge Lengths in High-Rise Concrete Shear Walls” *ACI Structural Journal*, Vol. 108, No. 2, March 2011, pp 148-157.

CHANG, G.A., MANDER, J.B., “Seismic Energy Based Fatigue Damage Analysis of Bridge Columns: Part

1–Evaluation of Seismic Capacity." NCEER Technical Report No. NCEER-94-0006, State University of New York, Buffalo, N.Y, June 1994, 164 Pages.

CHOPRA, Anil, "Dynamics of structures: Theory and application to earthquake engineering. 2nd ed. *Englewood Cliffs* (NJ, USA), Prentice Hall, Inc.; 2000.

COLEMAN, J. SPACONE, E., "Localization issues in forced-based frame elements", *Journal of Structural Engineering*, Vol. 127, No. 11, November 2001, pp 1257-1265.

EL-DAKHAKHNI, Wael, DRYSDALE, Robert, KHATTAB, Magdy, "Multilaminate Macromodel for Concrete Masonry: Formulation and Verification", *Journal of Structural Engineering*, Vol. 132, No. 12, December 2006, pp 1984-1996.

EZZELDIN, Mohamed, WIEBE, Lydell, SHEDID, Marwan, EL-DAKHAKHNI, Wael, "Numerical Modelling of Reinforced Concrete Block Structural Walls Under Seismic Loading." *9th International masonry conference*, Guimarães, Portugal, July 2014.

EZZELDIN, Mohamed, WIEBE, Lydell, EL-DAKHAKHNI, Wael, "Seismic Performance Assessment of Reinforced Masonry Walls With and Without Boundary Elements using the FEMA P695 Methodology." *Proceedings of the 12th North American masonry conference*, Denver, USA, May 2015.

GUINEA, G.V., HUSSEIN, G., ELICES, M., PLANAS, J., "Micromechanical Modelling of Brick-Masonry Fracture", *Cement Concrete Research*, Vol. 30, No. 5, May 2000, pp 731–737.

HOSE, Yael, SEIBLE, Frieder, "Performance Evaluation Database for Concrete Bridge Components and Systems Under Simulated Seismic Loads" *PEER report*. Berkley (USA), *Pacific Earthquake Engineering Research Center, College of Engineering*, University of California, November 1999.

LOURENÇO, Paulo, ROTS, Jan, "Multisurface Interface Model for Analysis of Masonry Structure", *Journal of Engineering Mechanics*, Vol. 123, No.7, July 1997, pp 660-668.

MANDER, J. B., PRIESTLEY, M. J. N., PARK, R., "Theoretical Stress-Strain Model for Confined Concrete", *Journal of Structural Engineering*, Vol. 114, No. 8, September 1988, pp 1804–1826.

RODRIGUEZ, Mario, BOTERO, Juan, VILLA, Jaime, "Cyclic Stress-Strain Behavior of Reinforcing Steel Including Effect of Buckling." *Journal of Structural Engineering,* Vol. 125, No. 6, June 1999, pp 605-612.

SHEDID, Marwan, EL-DAKHAKHNI, Wael, DRYSDALE, Robert, "Alternative Strategies to Enhance the Seismic Performance of Reinforced Concrete-Block Shear Wall Systems", *Journal of Structural Engineering*, Vol. 136, No. 6, June 2010, pp. 676-689.

STAVRIDIS, Andreas, SHING, P.P., "Finite-Element Modeling of Nonlinear Behavior of Masonry-Infilled RC Frames", *Journal of Structural Engineering*, Vol. 136, No. 3, March 2010, pp 285-296.

WAUGH, Jonathan, SRITHARAN, Sri, "Lessons Learned from Seismic Analysis of a Seven-Story Concrete Test Building", *Journal of Earthquake Engineering*, Vol. 14, No. 3, March 2010, pp 448-469.